

Field-induced spin nematic Tomonaga-Luttinger liquid of the $S=\frac{1}{2}$ spin ladder system with anisotropic ferromagnetic rung interaction

Tôru Sakai ^{1,2} Ryosuke Nakanishi,¹ Takaharu Yamada,¹ Rito Furuchi,¹ Hiroki Nakano,¹ Hirono Kaneyasu ¹, Kiyomi Okamoto,¹ and Takashi Tonegawa^{1,3,4}

¹Graduate School of Science, University of Hyogo, Kouto 3-2-1, Kamigori, Ako-gun, Hyogo 678-1297, Japan

²National Institute for Quantum Science and Technology (QST) SPring-8, Kouto 1-1-1, Sayo, Sayo-gun, Hyogo 679-5148, Japan

³Professor Emeritus, Kobe University, Kobe 657-8501, Japan

⁴Department of Physics, Graduate School of Science, Osaka Metropolitan University, Sakai 599-8531, Japan



(Received 12 April 2022; revised 11 August 2022; accepted 18 August 2022; published 29 August 2022)

The $S = \frac{1}{2}$ quantum spin ladder system with the anisotropic ferromagnetic exchange interaction on the rung under magnetic field is investigated using the numerical diagonalization and the density matrix renormalization group (DMRG) analyses. It is found that the nematic-spin-correlation-dominant Tomonaga-Luttinger liquid (TLL) appears in some high magnetic field. It is included in the TLL phase where the two-magnon bound state is realized. For some suitable parameters, after the field-induced phase transition from this two-magnon-bound TLL phase to the single-magnon TLL one, the re-entrant transition to the two-magnon-bound TLL phase occurs, which is confirmed by the magnetization curves by the DMRG. Several phase diagrams on the plane of the coupling anisotropy versus the magnetization and the magnetic field are presented. The present result is a proposal of the candidate system which exhibits the spin nematic phase without the biquadratic interaction or the frustration.

DOI: [10.1103/PhysRevB.106.064433](https://doi.org/10.1103/PhysRevB.106.064433)

I. INTRODUCTION

The spin nematic state [1,2] has attracted a lot of interest in the research field of the quantum spin systems and the strongly correlated electron systems. It is the long-range quadrupole order of spins by forming the two-magnon bound state. In the one-dimensional case, due to the strong quantum fluctuations, the nematic long-range order is reduced to the nematic quasi-long-range order, which should be called the spin nematic Tomonaga-Luttinger liquid (TLL). Namely, the quadrupole correlation function decays in the power-law in the spin nematic TLL phase.

It was shown that, in the $S = \frac{1}{2}$ ladder with different leg interactions and some anisotropies, two kinds of spin nematic TLL phases appeared, by using numerical diagonalization calculations, the density matrix renormalization group (DMRG) method, and perturbation calculations [3]. The spin nematic TLL phase was found in the simple $S = 1$ chain with the XXZ and on-site anisotropies [4–8]. The $S = 1$ bilinear and biquadratic chain was also theoretically predicted to exhibit the spin nematic TLL phase by several methods; the perturbation, [9] the bosonization, [10] the numerical exact diagonalization, [8,11] the field theory, [12] the DMRG [13], and the infinite matrix product state analysis [14]. Furthermore, the spin nematic TLL phase was revealed to occur in the $S = \frac{3}{2}$ bilinear and biquadratic model [9,15]. The spin frustration is another important mechanism to induce the spin nematic phase [16]. In order to explain the spin-liquid-like behavior of the $S = 1$ triangular magnet NiGa_2S_4 , [17] the spin nematic phase was proposed [18–21]. The frustrated spin chain

which has the ferromagnetic nearest- and the antiferromagnetic next-nearest-neighbor exchange interactions, are one of the popular models to exhibit the spin nematic TLL phase. The external magnetic field induced spin nematic TLL phase was predicted to occur in the $S = \frac{1}{2}$ chain with the ferromagnetic nearest- and the antiferromagnetic next-nearest-neighbor exchange interactions by the bosonization, [22] the numerical exact diagonalization, [23,24] the DMRG [24–26], and the field theory [26,27].

Several experimental methods to detect the spin nematic behavior were theoretically proposed, for example, the nuclear magnetic resonance (NMR), [28–32] the inelastic neutron scattering, [33] the μSR , [31], and the electron spin resonance (ESR) [34]. One of the suitable candidate materials to exhibit the spin nematic behavior is LiCuVO_4 which is the $S = \frac{1}{2}$ quasi-one-dimensional quantum spin system with the ferromagnetic nearest- and the antiferromagnetic next-nearest-neighbor exchange interactions [35]. The NMR measurements [35,36] on this compound under high magnetic field detected an evidence of the possible spin nematic order, as well as the magnetocaloric effect measurement [37]. The NMR experiment [38] on the similar compound LiCuSbO_4 [39] also observed the spin nematic order like behavior. Since the iron-based superconductors [40–44] were discovered, the spin nematic physics on the two dimensional systems [45–51] have been studied extensively, including the bilayer systems [52–54].

In most theories of the spin nematic behavior which have been proposed so far, the mechanism is based on the biquadratic interaction or the spin frustration. In this paper we

propose a simple theoretical model that exhibits the field-induced spin nematic TLL, without either the biquadratic interaction or the frustration. It is the $S = \frac{1}{2}$ spin ladder system with the anisotropic ferromagnetic rung exchange interaction under magnetic field. In previous work [55] the numerical diagonalization and the DMRG calculation indicated that the present model with the same amplitude between the antiferromagnetic leg and the ferromagnetic rung interactions gives rise to the field induced spin nematic TLL phase. In the present work the critical exponent analysis indicates that the spin nematic correlation dominant region and the spin density wave (SDW) correlation dominant region appear in the two-magnon-bound TLL phase. In addition we present several phase diagrams not only in the anisotropy-magnetization plane, but also in the anisotropy-external field plane, even for different amplitudes between the leg and rung interactions. The magnetization curves calculated by the DMRG are also presented for several typical cases.

II. MODEL

We consider the magnetization process of the $S = \frac{1}{2}$ Heisenberg spin ladder with the anisotropic ferromagnetic rung exchange interaction. The Hamiltonian is given by

$$\mathcal{H} = \mathcal{H}_0 + \mathcal{H}_Z, \quad (1)$$

$$\begin{aligned} \mathcal{H}_0 = & J_1 \sum_{\alpha=1}^2 \sum_{j=1}^L \mathbf{S}_{\alpha,j} \cdot \mathbf{S}_{\alpha,j+1} \\ & + J_r \sum_{j=1}^L [S_{1,j}^x S_{2,j}^x + S_{1,j}^y S_{2,j}^y + \lambda S_{1,j}^z S_{2,j}^z], \end{aligned} \quad (2)$$

$$\mathcal{H}_Z = -H \sum_{\alpha=1}^2 \sum_{j=1}^L S_{\alpha,j}^z, \quad (3)$$

where λ is an anisotropy parameter of the ferromagnetic rung exchange interaction and H is the external magnetic field. The ferromagnetic rung interaction constant J_r is set to be -1 . We consider the case of the antiferromagnetic leg interaction $J_1 > 0$ and the Ising-like anisotropy $\lambda > 1$ of the ferromagnetic rung interaction. For the length L system, the lowest energy of \mathcal{H}_0 in the subspace where $\sum_i \sum_j S_{i,j}^z = M$ is denoted by $E(L, M)$. The reduced magnetization m is defined by $m = M/M_s$, where M_s denotes the saturation of the magnetization, namely $M_s = L$. The energies $E(L, M)$ are calculated by the Lanczos algorithm under the periodic boundary condition ($\mathbf{S}_{i,L+1} = \mathbf{S}_{i,1}$).

III. HALDANE-NEEL PHASE BOUNDARY

In the absence of the external field ($H = 0$), the ground state of the system is in the Haldane phase with the Haldane gap for $\lambda \sim 1$, while in the Néel ordered phase for $\lambda \gg 1$. The phase boundary λ_c can be estimated using the phenomenological renormalization group method [56]. The size-dependent critical point $\lambda_{c,L+1}$ is determined from the equation of the scaled gaps

$$L\Delta_\pi(L, \lambda_c) = (L+2)\Delta_\pi(L+2, \lambda_c), \quad (4)$$

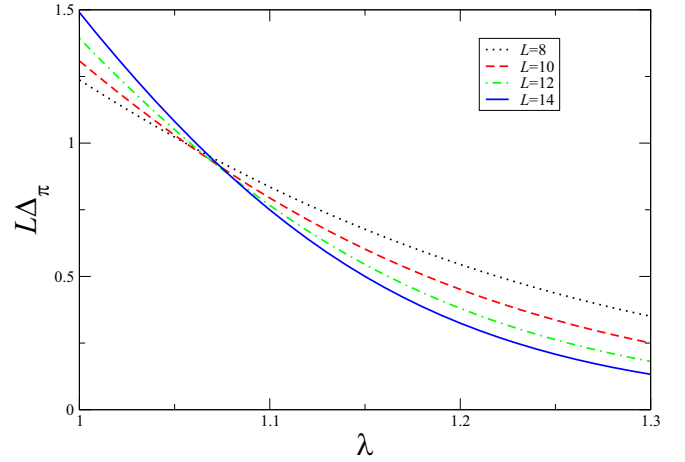


FIG. 1. Scaled gap $L\Delta_\pi(L, \lambda)$ plotted versus λ for $L = 8, 10, 12$ and 14 in the case of $J_1 = 0.5$.

where $\Delta_\pi(L, \lambda)$ is the lowest excitation gap with the wave number $k = \pi$. The scaled gap $L\Delta_\pi(L, \lambda)$ is plotted versus λ for $L = 8, 10, 12$ and 14 in the case of $J_1 = 0.5$ shown in Fig. 1. Assuming the size correction proportional to $1/L$, we estimate the phase boundary λ_c in the infinite length limit as shown in Fig. 2.

IV. TWO TOMONAGA-LUTTINGER LIQUID PHASES

If the magnetization process begins from the Haldane phase for $\lambda < \lambda_c$, a quantum phase transition would occur at the critical field H_{c1} where the spin gap vanishes, and the gapless TLL phase would appear for $H > H_{c1}$, like the $S = 1$ antiferromagnetic chain [57–61]. This TLL phase is called the conventional TLL (CTLL) phase where each step of the magnetization curve for the finite-size systems should be $\delta M = \delta S_{\text{tot}}^z = 1$. On the other hand, starting from the Néel ordered phase for $\lambda > \lambda_c$, the large Ising-like anisotropy stabilizes the states $|\uparrow\uparrow\rangle$ and $|\downarrow\downarrow\rangle$ at each rung pair, which is nothing but the local two-magnon bound state. These

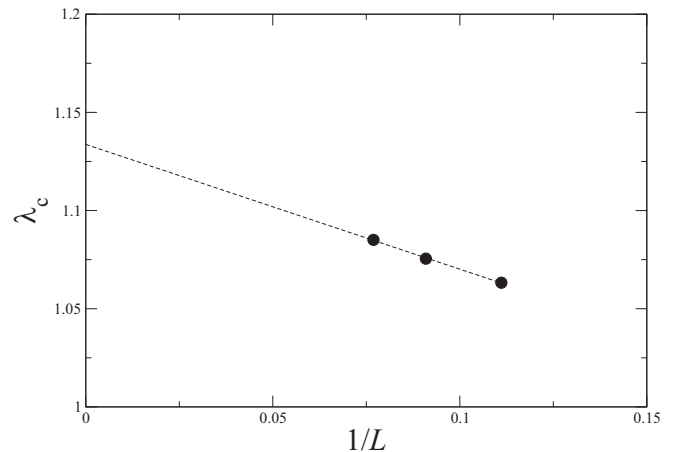


FIG. 2. Extrapolation of the Néel-Haldane boundary at $m = 0$ for $J_1 = 0.5$. We can see that $\lambda_{c,N+1}$ converges as $1/L$. The extrapolated value is $\lambda_c = 1.134 \pm 0.002$.

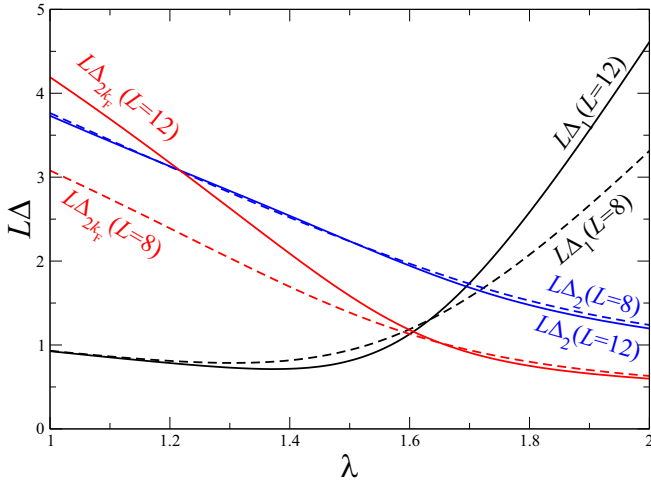


FIG. 3. Scaled gaps $L\Delta_1$ (black curves), $L\Delta_2$ (blue curves) and $L\Delta_{2k_F}$ (red curves) plotted versus λ for $L = 8$ (dashed curves) and 12 (solid curves) in case of $J_1 = 0.5$ and $m = 1/2$.

two states can be expressed by the $T = 1/2$ pseudo-spin with $|T^z = +1\rangle = |\uparrow\uparrow\rangle$ and $|T^z = -1\rangle = |\downarrow\downarrow\rangle$. Then the magnetization process will be similar to the Ising-like $T = 1/2$ XXZ single antiferromagnetic chain. This TLL phase is called the two-magnon-bound TLL phase, where each step of the magnetization curve should be $\delta M = 2$. The gapless quasiparticle excitation is different between these two TLL phases. Namely, it is the single magnon excitation for the CTLL, while it is the two-magnon excitation for the two-magnon-bound TLL. We note that the single magnon excitation is gapped in the two-magnon-bound TLL. Thus the cross points between these two excitation gaps given by the forms

$$\Delta_1 = E(L, M + 1) + E(M - 1) - 2E(M), \quad (5)$$

$$\Delta_2 = E(L, M + 2) + E(L, M - 2) - 2E(M), \quad (6)$$

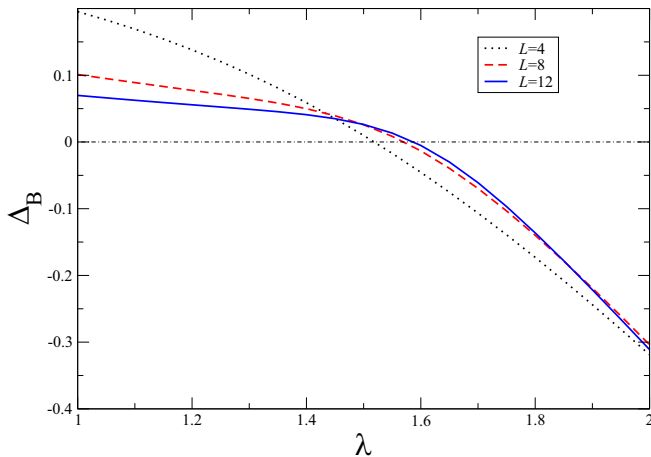


FIG. 4. Two-magnon binding energies Δ_B are plotted versus λ for $J_1 = 0.5$ and $m = 1/2$.

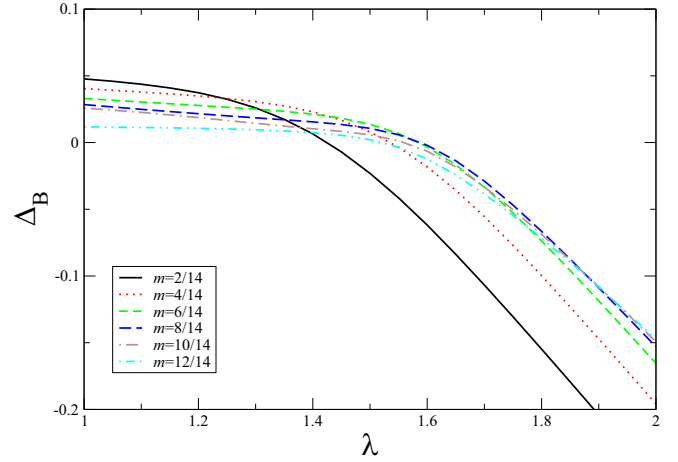


FIG. 5. Two-magnon binding energies Δ_B as functions of λ for various M in case of $J_1 = 0.5$ and $L = 14$.

will be the phase boundary λ_c in the infinite L limit for each magnetization M . At the half of the saturation magnetization $m = 1/2$ for $J_1 = 0.5$, the scaled gaps $L\Delta_1$ (black curves) and $L\Delta_2$ (blue curves) are plotted versus λ for $L = 8$ (dashed curves) and 12 (solid curves), respectively in Fig. 3. It indicates that Δ_1 is gapless for smaller λ but gapped for larger λ , while Δ_2 is always gapless.

Considering the gapless $2k_F$ excitation, we can use another method to estimate the phase boundary. Since the wave number $2k_F$ is different between two TLL phases, this excitation in the two-magnon-bound TLL phase ($2k_F = 2m\pi$) is gapped in the CTLL phase, while gapless in the two-magnon-bound TLL phase. Thus the behaviors of the $2k_F$ excitation gap for the two-magnon-bound TLL phase Δ_{2k_F} and Δ_1 are just switched at the critical point. The scaled gap $L\Delta_{2k_F}$ (red curve) is also plotted versus λ for $L = 8$ and 12 in Fig. 3. The cross

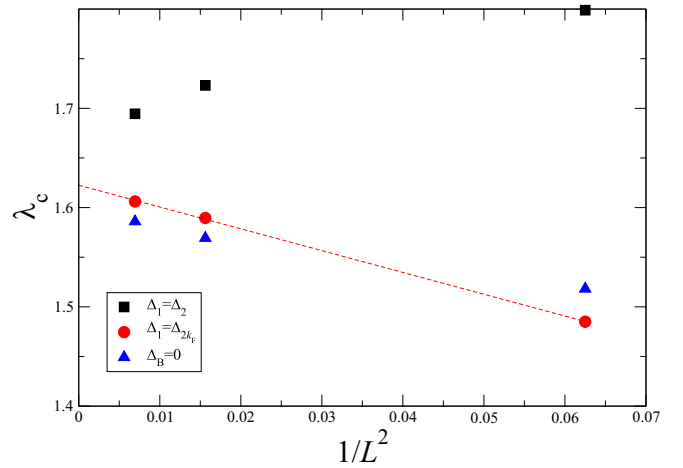


FIG. 6. The cross points between Δ_1 and Δ_2 (black squares), and those between Δ_1 and Δ_{2k_F} (red circles) are plotted versus $1/L^2$ in the case of $J_1 = 0.5$ and $m = 1/2$. The points where $\Delta_B = 0$ are also plotted (blue triangles). The first and third points converge as $1/L$, whereas the second points as $1/L^2$. The $L \rightarrow \infty$ extrapolated value of the second points is $\lambda_c = 1.623 \pm 0.002$.

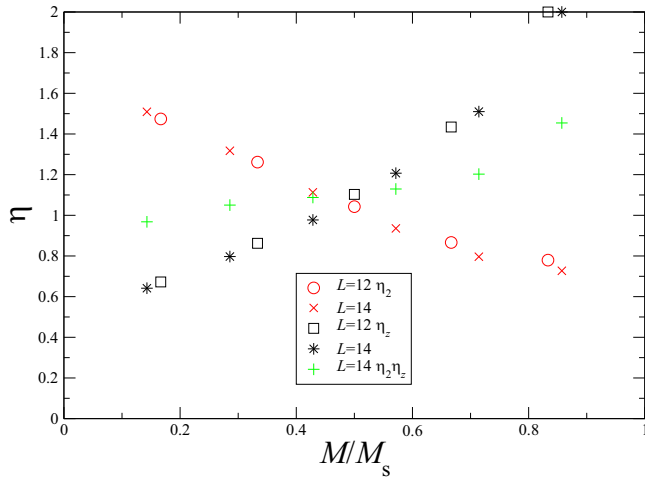


FIG. 7. Critical exponents η_z and η_2 for $L = 12$ and 14 are plotted versus M/M_s for $J_1 = 0.5$ and $\lambda = 2.5$. The product $\eta_2 \eta_z$ is also plotted for $L = 14$.

point of Δ_1 and Δ_{2k_F} would be also the phase boundary λ_c in the infinite L limit.

We also calculate the two-magnon binding energy [62] defined by

$$\begin{aligned} \Delta_B &= \{E(L, M+2) - E(L, M)\} \\ &\quad - 2\{E(L, M+1) - E(L, M)\} \\ &= E(L, M) + E(L, M+2) - 2E(L, M+1), \end{aligned} \quad (7)$$

which should be positive in the CTLL phase while negative in the two-magnon-bound TLL phase. Therefore the point $\Delta_B = 0$ would be the phase transition point in the $L \rightarrow \infty$ limit. The behavior of Δ_B for $J_1 = 0.5$ and $m = 1/2$ is shown in

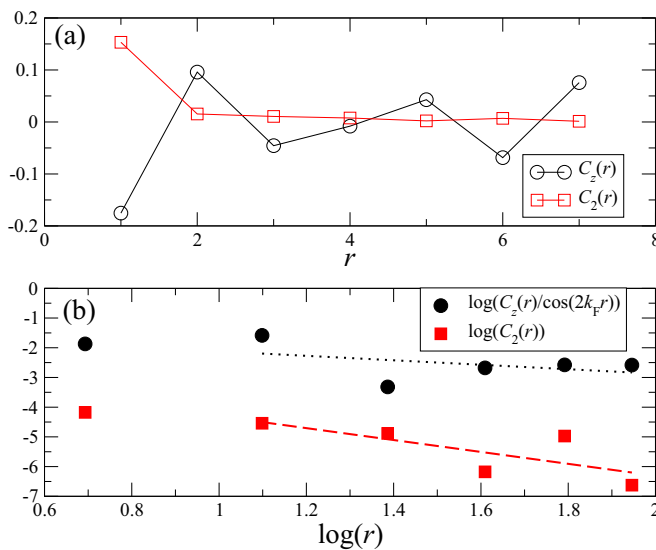


FIG. 8. Behaviors of $C_z(r)$ and $C_2(r)$ in the case of $J_1 = 0.5$, $\lambda = 2.5$ and $m = 2/14$ in the SDW_2 TLL region. The dotted and dashed lines in (b) are guide for the eye. We see that $C_z(r)$ is predominant over $C_2(r)$.

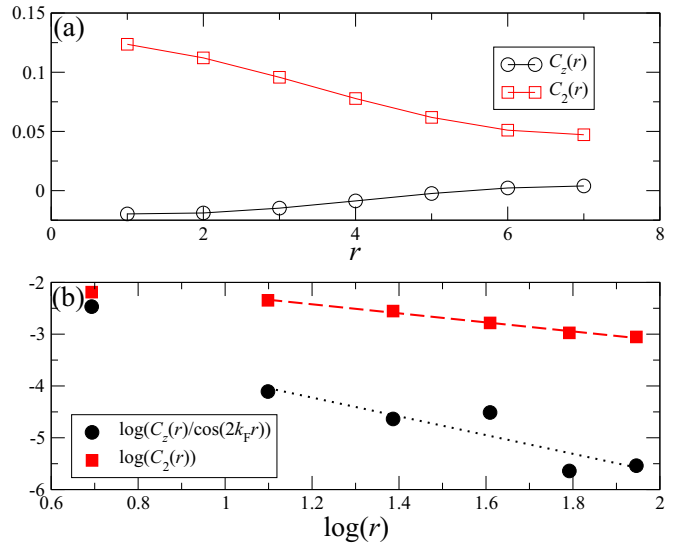


FIG. 9. Behaviors of $C_z(r)$ and $C_2(r)$ in the case of $J_1 = 0.5$, $\lambda = 2.5$ and $m = 10/14$ in the NTLT region. The dotted and dashed lines in (b) are guide for the eye. We see that $C_2(r)$ is predominant over $C_z(r)$.

Fig. 4. We also show the binding energies as functions of λ for various M in case of $J_0 = 0.5$ and $L = 14$ in Fig. 5.

The behaviors of the gaps and the two-magnon binding energy are most basic properties to distinguish the CTLL and two-magnon-bound TLL phases. Thus the phase transition between these two phases is directly confirmed by Figs. 3 and 4. The cross points of Δ_1 and Δ_2 (black squares), and that of Δ_1 and Δ_{2k_F} (red circles) as well as the points $\Delta_B = 0$ (blue triangles) for $L = 4, 8$, and 12 are plotted versus $1/L^2$ in Fig. 6. The first and third points converges with respect to L almost as $1/L$, while the second ones almost as $1/L^2$. Since the phase boundary depends on the magnetization M , we use the cross point of Δ_1 and Δ_{2k_F} for largest L as the phase boundary at each M .

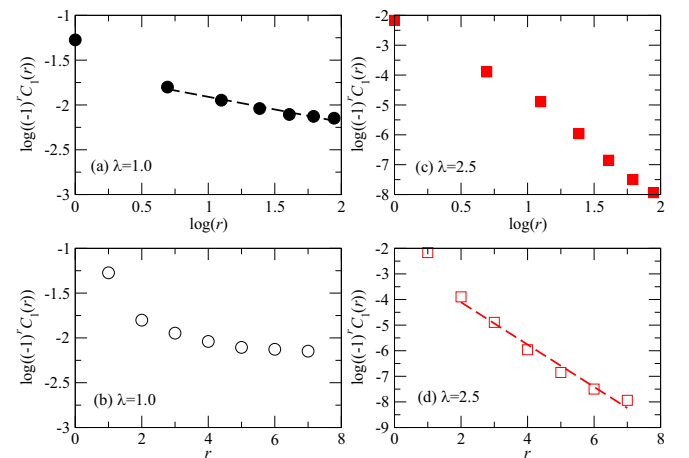


FIG. 10. (a)(b) Behavior of $C_1(r)$ in case of $J_1 = 0.5$, $\lambda = 1.0$, and $m = 2/14$ in the CTLL phase. (c)(d) Behavior of $C_1(r)$ in case of $J_1 = 0.5$, $\lambda = 2.5$, and $m = 2/14$ in the SDW_2 TLL region. The broken lines are guide for the eye.

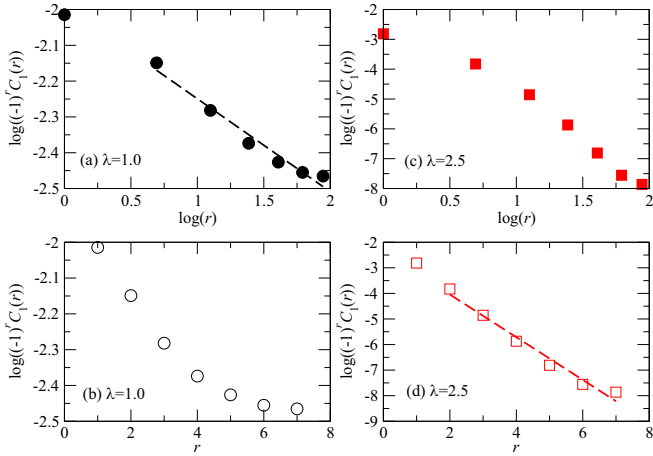


FIG. 11. (a)(b) Behavior of $C_1(r)$ in the case of $J_1 = 0.5$, $\lambda = 1.0$, and $m = 10/14$ in the CTLL phase. (c), (d) Behavior of $C_1(r)$ in case of $J_1 = 0.5$, $\lambda = 2.5$, and $m = 10/14$ in the NTLL region. The dashed lines are guide for the eye.

V. SPIN CORRELATIONS

In the two-magnon-bound TLL phase the following spin correlation functions exhibit the power-law decay:

$$C_z(r) \equiv \langle S_{\alpha,0}^z S_{\alpha,r}^z \rangle - \langle S^z \rangle^2 \sim \cos(2k_F r) r^{-\eta_z}, \quad (8)$$

$$C_2(r) \equiv \langle S_{1,0}^+ S_{2,0}^+ S_{1,r}^- S_{2,r}^- \rangle \sim r^{-\eta_2}. \quad (9)$$

The former corresponds to the SDW spin correlation parallel to the external field and the latter corresponds to the nematic (quadrupole) spin correlation perpendicular to the external field. Comparing the exponents η_z and η_2 , the smaller determines the dominant spin correlation. The area for $\eta_2 < \eta_z$ in the parameter space should be called the nematic correlation dominant TLL (NTLL) region, and that for $\eta_2 > \eta_z$ the SDW dominant TLL (SDW₂TLL) region. According to the

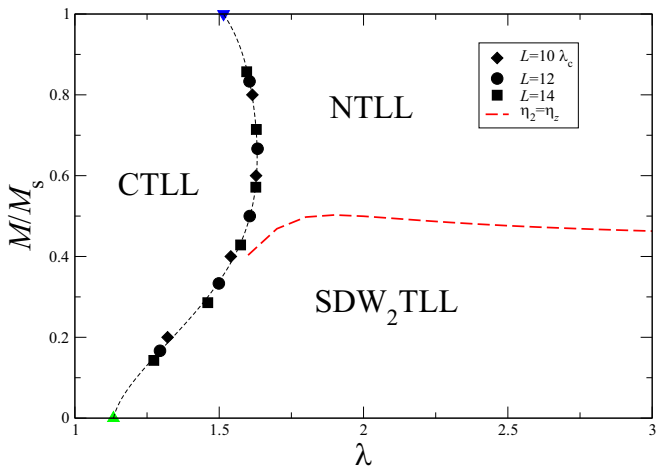


FIG. 12. Phase diagram with respect to the anisotropy and the magnetization for $J_1 = 0.5$. For the green triangle \blacktriangle and blue triangle \blacktriangledown , see the text.

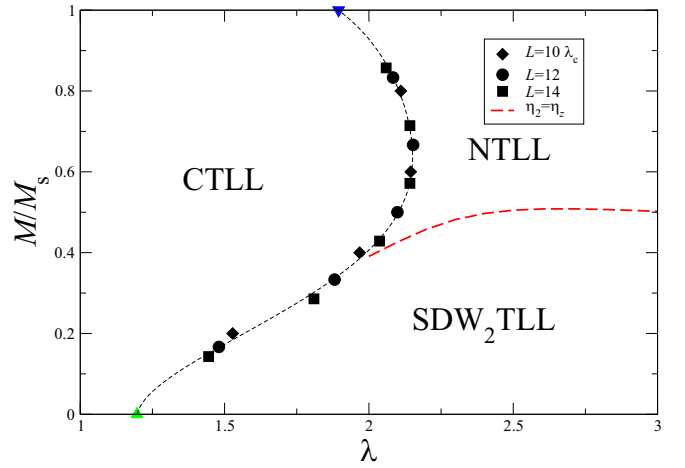


FIG. 13. Phase diagram with respect to the anisotropy and the magnetization for $J_1 = 1.0$.

conformal field theory, these exponents can be estimated by the forms

$$\eta_2 = \frac{E(L, M+2) + E(L, M-2) - 2E(L, M)}{E_{k_1}(L, M) - E(L, M)}, \quad (10)$$

$$\eta_z = 2 \frac{E_{2k_F}(L, M) - E(L, M)}{E_{k_1}(L, M) - E(L, M)}, \quad (11)$$

for each magnetization M , where k_1 is defined as $k_1 = L/2\pi$. The exponents η_2 and η_z estimated for $L=12$ and 14 are plotted versus M/M_s for $J_1 = 0.5$ and $\lambda = 2.5$ in Fig. 7. It suggests that the SDW correlation is dominant for small M , while the nematic one for large M . Since the cross point of η_2 and η_z is not so strongly dependent on L , the cross point of $L = 14$ is used as the crossover point between the NTLL and SDW₂TLL regions. The product of $\eta_2 \eta_z$ is also plotted in Fig. 7. The characteristic condition of the TLL theory $\eta_2 \eta_z = 1$ is well satisfied around the cross point.

We show the behaviors of $C_z(r)$ and $C_2(r)$ in Figs. 8 and 9. As already stated, $C_z(r)$ is predominant over $C_2(r)$ in the

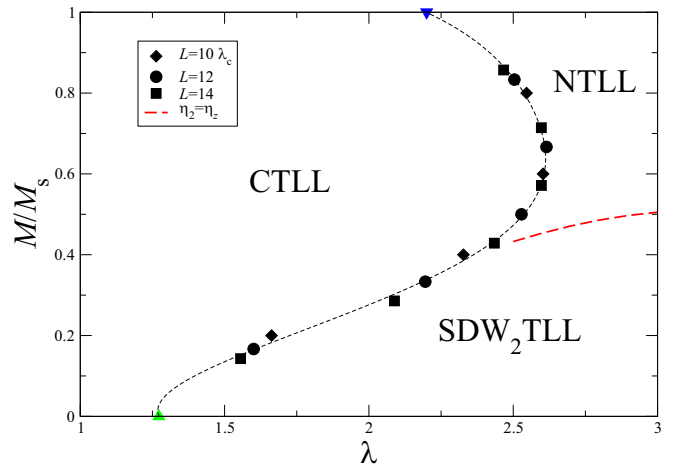


FIG. 14. Phase diagram with respect to the anisotropy and the magnetization for $J_1 = 1.5$.

TABLE I. Result of the Shanks transformation applied to the sequence $H_{c2} = [E(L, 2) - E(L, 0)]/2$ twice for $J_1 = 0.5$ and $\lambda = 2.0$.

L	P_L	P'_L	P''_L
6	0.4320515		
8	0.4138989	0.3920970	
10	0.4039936	0.3873292	0.3832358
12	0.3977810	0.3851267	
14	0.3936142		

SDW₂TLL region and vice versa in the NTLL region. We can see that this situation is realized in Figs. 8 and 9, although the precise determination of the critical exponents η_z and η_2 is difficult. Thus we think that these figures provide the direct confirmation of the difference between the SWD₂TLL and NTLL regions.

We also calculate the two-spin correlation function defined by

$$C_1(r) \equiv \langle S_{\alpha,0}^+ S_{\alpha,r}^- \rangle, \quad (12)$$

which is expected to decay in the power law in the CTLL phase while in the exponential law in the two-magnon bound TLL phase. The behavior of $C_1(r)$ is shown in Figs. 10 and 11. In both figures the magnitudes of $C_1(r)$ are much larger in the CTLL phase than in the two-magnon bound TLL phase (SDW₂TLL and NTLL regions). Also the decay patterns of $C_1(r)$ are consistent with the above expectation. Therefore Figs. 10 and 11 provide the direct confirmation of the phase transition between the CTLL phase and the two-magnon bound TLL phase.

VI. PHASE DIAGRAMS

Now we present several phase diagrams including the field-induced NTLL and SDW₂TLL regions. At first the phase diagrams on the plane of the anisotropy λ and the reduced magnetization $m = M/M_s$ for $J_1=0.5, 1.0$ and 1.5 are shown

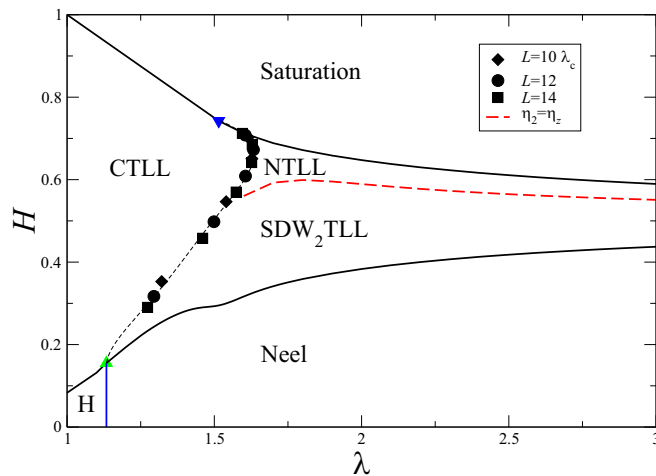


FIG. 15. Phase diagram with respect to the anisotropy and the magnetic field for $J_1 = 0.5$. The phase denoted by H is the Haldane phase.

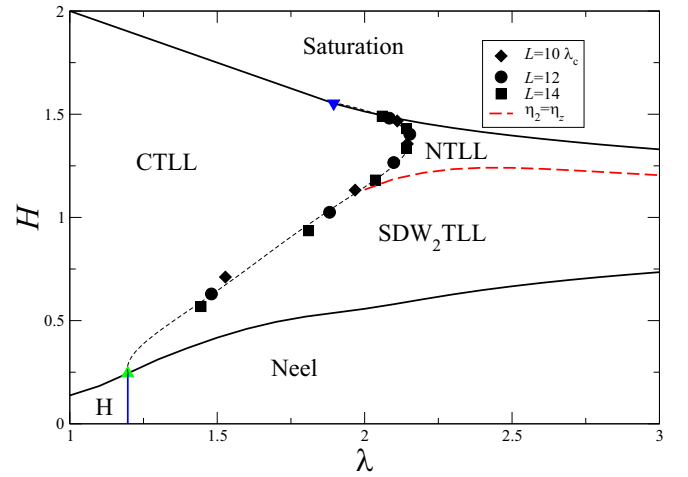


FIG. 16. Phase diagram with respect to the anisotropy and the magnetic field for $J_1 = 1.0$.

in Figs. 12–14, respectively. The phase boundary between the CTLL and the two-magnon-bound TLL phases is obtained as the cross of Δ_1 and Δ_{2k_F} at each M for $L=10$ (diamond), 12 (circle) and 14 (square). The two-magnon-bound TLL phase is divided into the NTLL and SDW₂TLL regions by the crossover line (broken red curve) determined by $\eta_2 = \eta_z$. The critical point between the Haldane and Néel phases at $M=0$ determined by the phenomenological renormalization group method is given as a green triangle \blacktriangle . The phase boundary (blue triangle \blacktriangledown) at $m = M/M_s = 1$ is the point where the saturation field changes from $H_{s1} = E(L, L) - E(L, L-1)$ to $H_{s2} = [E(L, L) - E(L, L-2)]/2$, which is almost independent of L . The dashed curve is the guide for the eye for the phase boundary between CTLL and the two-magnon-bound TLL phases.

The phase diagrams with respect to the external magnetic field H would be much more useful for experimentalists. The external field H giving the magnetization M is estimated by

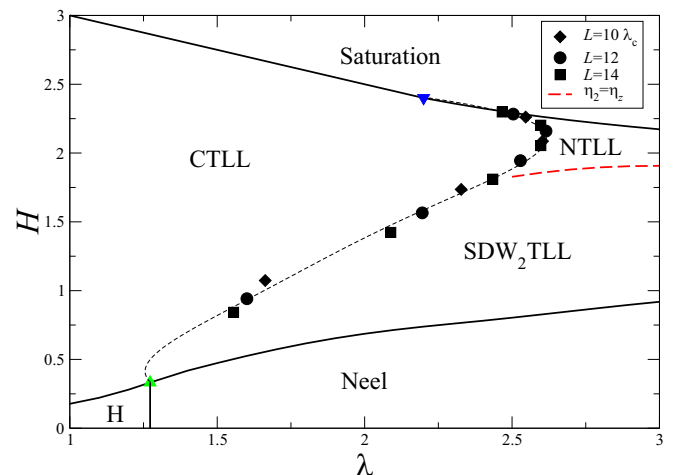


FIG. 17. Phase diagram with respect to the anisotropy and the magnetic field for $J_1 = 1.5$.

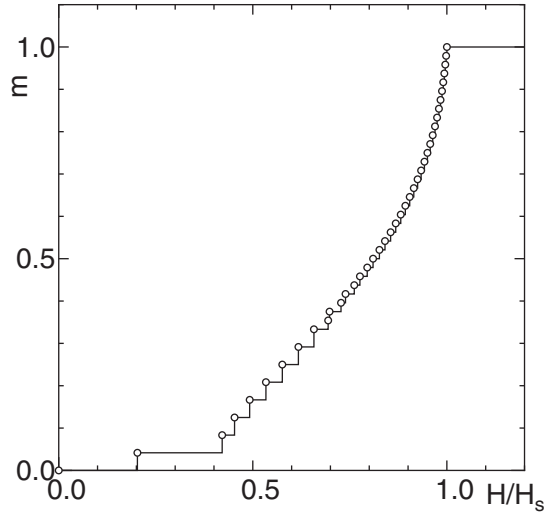


FIG. 18. Magnetization curve obtained by the DMRG for $J_1 = 0.5$ and $\lambda = 1.50$.

the form

$$H = [E(L, M + 1) - E(L, M - 1)]/2 \quad (13)$$

at each phase boundary and by the form

$$H = [E(L, M + 2) - E(L, M - 2)]/4 \quad (14)$$

at each crossover point. The phase boundary between the Haldane (H) and CTLL phases is estimated by the Shanks transformation [63,64] applied to the critical field $H_{c1}^{(1)}$ given by

$$H_{c1}^{(1)} = E(L, 1) - E(L, 0) \quad (15)$$

calculated for $L = 6, 8, 10, 12$, and 14 . The boundary between the Néel and the two-magnon-bound TLL phases is estimated by the same method applied to $H_{c1}^{(2)}$ given by

$$H_{c1}^{(2)} = [E(L, 2) - E(L, 0)]/2. \quad (16)$$

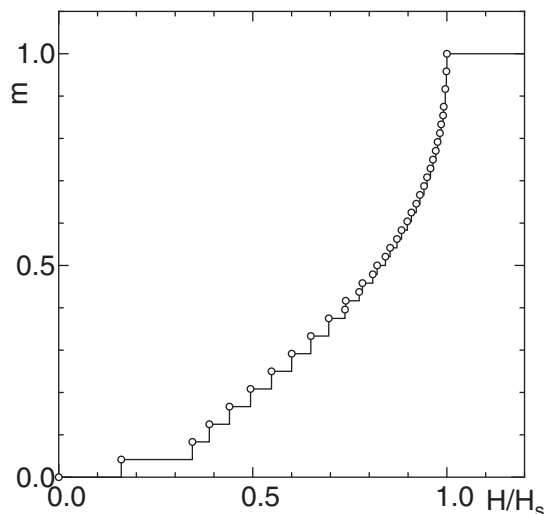


FIG. 19. Magnetization curve obtained by the DMRG for $J_1 = 0.5$ and $\lambda = 1.55$.

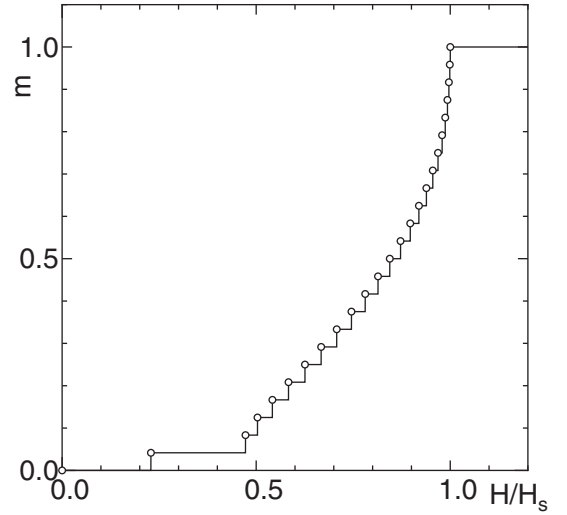


FIG. 20. Magnetization curve obtained by the DMRG for $J_1 = 0.5$ and $\lambda = 1.60$.

The Shanks transformation applied to a sequence $\{P_L\}$ is defined as the form

$$P'_L = \frac{P_{L-2}P_{L+2} - P_L^2}{P_{L-2} + P_{L+2} - 2P_L}. \quad (17)$$

The result of this transformation applied to H_{c2} for $J_1 = 0.5$ and $\lambda = 2.0$ is shown in Table I. The phase diagrams in the λ - H plane for $J_1 = 0.5, 1.0$, and 1.5 are shown in Figs. 15–17, respectively. In all the cases the NTLL region appears only in the magnetization process from the Néel ordered phase.

VII. MAGNETIZATION CURVES

The magnetization curves are calculated by the DMRG method for $L = 96$ under the open boundary condition with fixed $J_1 = 0.5$ for $\lambda = 1.50, 1.55$ and 1.60 shown in Figs. 18–20, respectively. The region with $\delta M = 1$ corresponds to the CTLL phase, while that with $\delta M = 2$ the two-magnon-bound TLL phase. These three magnetization curves are consistent with the phase diagrams in Figs. 12 and 15. In Fig. 18 the field-induced transition from SDW_2TLL to CTLL phases occurs at $H/H_s \sim 0.7$. In Fig. 19 the first transitions from the SDW_2TLL to the CTLL phases occurs at $H/H_s \sim 0.7$ and the second one to the NTLL phase appears just before the saturation. In Fig. 20 the crossover from the SDW_2TLL to the NTLL regions is expected to occur, which does not bring about any change of the magnetization step. At any field induced transition or crossover, the magnetization curve does not exhibit any significant anomalous behavior, such as the magnetization plateau, jump, or kink etc.

VIII. DISCUSSION

In order to propose the experiments to observe the field induced NTLL phase, we should look for the $S = \frac{1}{2}$ spin ladder systems with the ferromagnetic rung interaction. Possible candidate materials are as follows: $(CH_3)_2CHNH_3CuCl_3$, [65–70] $Li_2Cu_2O(SO_4)_2$ [71] and the organic spin ladder 3-I-V[3-(3-iodophenyl)-1,5-diphenylverdazyl] [72]. Among three

compounds the first and the second ones were revealed to have the spin gap which suggests the Haldane state at zero magnetic field. Thus they have no chance to observe the NTLL. On the other hand, for the third one the Néel order was observed at $H = 0$ and a kind of multipolar order was observed near the saturation of the magnetization process. Some more extensive analyses on this material would be interesting.

In order to detect the spin nematic TLL phase, the NMR measurement is one of suitable methods. The critical exponent of the spin correlation function η_z calculated in the Sec. V can be estimated from the temperature dependence of the NMR relaxation rate [28,29]. The region for $\eta_z > 1$ at low temperature is expected to be in the spin nematic TLL phase. Actually the spin nematic behavior of the frustrated spin chain compound LiCuSbO_4 was observed by this experimental method [73]. The NMR measurement on some spin ladder materials would be also quite interesting. Furuya [74] showed that a characteristic angular dependence of the linewidth of the paramagnetic resonance peak in the ESR absorption spectrum occurred in the two-magnon-bound TLL phase. This experiment is also strongly desirable.

IX. SUMMARY

The $S = \frac{1}{2}$ spin ladder system with the anisotropic ferromagnetic rung interaction under magnetic field is investigated using the numerical diagonalization for finite-size clusters and the DMRG analyses. The critical exponent analysis reveals that, in the field-induced two-magnon-bound TLL phase, the NTLL region appears for large H , while the SDW_2TLL one for small H . The magnetization curves calculated by the DMRG indicates that after the field-induced phase transition from the SDW_2TLL to the CTLL phases, the transition to the NTLL phase would possibly occur, for some suitable parameters. Several phase diagrams with respect to the coupling anisotropy, the magnetization, and the magnetic field

are presented. It would be a good proposal of the candidate system that exhibits the field-induced spin nematic liquid phase, without the frustration or the biquadratic exchange interaction.

The field-induced nematic liquid phase in the unfrustrated system has been found in $S = 1$ models [8,75] and the $S = \frac{1}{2}$ ladder model with ferromagnetic rung interactions [55]. The key point for the realization of the field-induced nematic liquid phase in the former models is the easy-axis on-site anisotropy which chooses the $|S^z = \pm 1\rangle$ states over the $|S^z = 0\rangle$ state. For the latter model the key point is the Ising-like XXZ anisotropy of the ferromagnetic bond which prefers the $|\uparrow\uparrow\rangle$ and $|\downarrow\downarrow\rangle$ states to the $(1/\sqrt{2})|\uparrow\downarrow \pm \downarrow\uparrow\rangle$ states of the spin pair connected by the ferromagnetic interaction. These key points are essentially the same as each other as can be seen by mapping the latter model onto the $S = 1$ model. Thus the field-induced nematic liquid phase is expected in models in which the above key point is satisfied. In fact, recently we have found the field-induced nematic liquid phase in the $S = \frac{1}{2}$ ferromagnetic-antiferromagnetic bond-alternating chain [76] and in the $S = \frac{1}{2}$ Δ -chain with ferromagnetic interactions [77].

ACKNOWLEDGMENTS

This work was partly supported by JSPS KAKENHI, Grants No. JP16K05419, No. JP20K03866, No. JP16H01080 (J-Physics), No. JP18H04330 (J-Physics) and No. JP20H05274. A part of the computations was performed using facilities of the Supercomputer Center, Institute for Solid State Physics, University of Tokyo, and the Computer Room, Yukawa Institute for Theoretical Physics, Kyoto University. We used the computational resources of the supercomputer Fugaku provided by the RIKEN through the HPCI System Research projects (Project ID: hp200173, hp210068, hp210127, hp210201, and hp220043).

-
- [1] A. F. Andreev and A. Grishchuk, *Sov. Phys. JETP* **60**, 267 (1984).
 - [2] H. H. Chen and P. M. Levy, *Phys. Rev. Lett.* **27**, 1383 (1971).
 - [3] T. Tonegawa, T. Hikihara, K. Okamoto, S. C. Furuya, and T. Sakai, *J. Phys. Soc. Jpn.* **87**, 104002 (2018).
 - [4] J. Sólyom and T. A. L. Ziman, *Phys. Rev. B* **30**, 3980 (1984).
 - [5] H. J. Schulz, *Phys. Rev. B* **34**, 6372 (1986).
 - [6] M. den Nijs and K. Rommelse, *Phys. Rev. B* **40**, 4709 (1989).
 - [7] W. Chen, K. Hida, and B. C. Sanctuary, *Phys. Rev. B* **67**, 104401 (2003).
 - [8] T. Sakai, H. Nakano, R. Furuchi, and K. Okamoto, *J. Phys.: Conf. Ser.* **2164**, 012030 (2022).
 - [9] A. V. Chubukov, *J. Phys.: Condens. Matter* **2**, 1593 (1990).
 - [10] G. Fáth and J. Sólyom, *Phys. Rev. B* **51**, 3620 (1995).
 - [11] A. Läuchli, G. Schmid, and S. Trebst, *Phys. Rev. B* **74**, 144426 (2006).
 - [12] T. Grover and T. Senthil, *Phys. Rev. Lett.* **98**, 247202 (2007).
 - [13] S. R. Manmana, A. M. Läuchli, F. H. L. Essler, and F. Mila, *Phys. Rev. B* **83**, 184433 (2011).
 - [14] R. M. Mao, Y.-W. Dai, S. Y. Cho, and H.-Q. Zhou, *Phys. Rev. B* **103**, 014446 (2021).
 - [15] Y. A. Fridman, O. A. Kosmachev, A. K. Kolezhuk, and B. A. Ivanov, *Phys. Rev. Lett.* **106**, 097202 (2011).
 - [16] P. Chandra and P. Coleman, *Phys. Rev. Lett.* **66**, 100 (1991).
 - [17] S. Nakatsuji, Y. Nambu, H. Tonomura, O. Sakai, S. Jonas, C. Broholm, H. Tsunetsugu, Y. Qiu, and Y. Maeno, *Science* **309**, 1697 (2005).
 - [18] H. Tsunetsugu and M. Arikawa, *J. Phys. Soc. Jpn.* **75**, 083701 (2006).
 - [19] A. Läuchli, F. Mila, and K. Penc, *Phys. Rev. Lett.* **97**, 087205 (2006).
 - [20] S. Bhattacharjee, V. B. Shenoy, and T. Senthil, *Phys. Rev. B* **74**, 092406 (2006).
 - [21] J.-H. Park, S. Onoda, N. Nagaosa, and J. H. Han, *Phys. Rev. Lett.* **101**, 167202 (2008).
 - [22] A. V. Chubukov, *Phys. Rev. B* **44**, 4693 (1991).
 - [23] T. Vekua, A. Honecker, H.-J. Mikeska, and F. Heidrich-Meisner, *Phys. Rev. B* **76**, 174420 (2007).

- [24] J. Sudan, A. Lüscher, and A. M. Läuchli, *Phys. Rev. B* **80**, 140402(R) (2009).
- [25] T. Hikihara, L. Kecke, T. Momoi, and A. Furusaki, *Phys. Rev. B* **78**, 144404 (2008).
- [26] M. Sato, T. Hikihara, and T. Momoi, *Phys. Rev. Lett.* **110**, 077206 (2013).
- [27] O. A. Starykh and L. Balents, *Phys. Rev. B* **89**, 104407 (2014).
- [28] M. Sato, T. Momoi, and A. Furusaki, *Phys. Rev. B* **79**, 060406(R) (2009).
- [29] M. Sato, T. Hikihara, and T. Momoi, *Phys. Rev. B* **83**, 064405 (2011).
- [30] R. Shindou, S. Yunoki, and T. Momoi, *Phys. Rev. B* **87**, 054429 (2013).
- [31] A. Smerald and N. Shannon, *Phys. Rev. B* **88**, 184430 (2013).
- [32] A. Smerald and N. Shannon, *Phys. Rev. B* **93**, 184419 (2016).
- [33] A. Smerald, H. T. Ueda, and N. Shannon, *Phys. Rev. B* **91**, 174402 (2015).
- [34] S. C. Furuya and T. Momoi, *Phys. Rev. B* **97**, 104411 (2018).
- [35] N. Büttgen, K. Nawa, T. Fujita, M. Hagiwara, P. Kuhns, A. Prokofiev, A. P. Reyes, L. E. Svistov, K. Yoshimura, and M. Takigawa, *Phys. Rev. B* **90**, 134401 (2014).
- [36] A. Orlova, E. L. Green, J. M. Law, D. I. Gorbunov, G. Chanda, S. Krämer, M. Horvatić, R. K. Kremer, J. Wosnitza and G. L. J. A. Rikken, *Phys. Rev. Lett.* **118**, 247201 (2017).
- [37] M. Gen, T. Nomura, D. I. Gorbunov, S. Yasin, P. T. Cong, C. Dong, Y. Kohama, E. L. Green, J. M. Law, M. S. Henriques, J. Wosnitza, A. A. Zvyagin, V. O. Chervanovskii, R. K. Kremer, and S. Zherlitsyn, *Phys. Rev. Research* **1**, 033065 (2019).
- [38] M. Bosiočić, F. Bert, S. E. Dutton, R. J. Cava, P. J. Baker, M. Požek, and P. Mendels, *Phys. Rev. B* **96**, 224424 (2017).
- [39] S. E. Dutton, M. Kumar, M. Mourigal, Z. G. Soos, J.-J. Wen, C. L. Broholm, N. H. Andersen, Q. Huang, M. Zbiri, R. Toft-Petersen, and R. J. Cava, *Phys. Rev. Lett.* **108**, 187206 (2012).
- [40] Y. Kamihara, T. Watanabe, M. Hirano, and H. Hosono, *J. Am. Chem. Soc.* **130**, 3296 (2008).
- [41] G. R. Stewart, *Rev. Mod. Phys.* **83**, 1589 (2011).
- [42] Q. Si, R. Yu, and E. Abrahams, *Nat. Rev. Mater.* **1**, 16017 (2016).
- [43] P. Dai, J. Hu, and E. Dagotto, *Nat. Phys.* **8**, 709 (2012).
- [44] E. Dagotto, *Rev. Mod. Phys.* **85**, 849 (2013).
- [45] A. Läuchli, J. C. Domenge, C. Lhuillier, P. Sindzingre, and M. Troyer, *Phys. Rev. Lett.* **95**, 137206 (2005).
- [46] N. Shannon, T. Momoi, and P. Sindzingre, *Phys. Rev. Lett.* **96**, 027213 (2006).
- [47] S. Capponi and F. F. Assaad, *Phys. Rev. B* **75**, 045115 (2007).
- [48] R. Shindou and T. Momoi, *Phys. Rev. B* **80**, 064410 (2009).
- [49] L. W. Harriger, H. Q. Luo, M. S. Liu, C. Frost, J. P. Hu, M. R. Norman, and P. Dai, *Phys. Rev. B* **84**, 054544 (2011).
- [50] W.-J. Hu, H.-H. Lai, S.-S. Gong, R. Yu, E. Dagotto, and Q. Si, *Phys. Rev. Research* **2**, 023359 (2020).
- [51] K. Tanaka and C. Hotta, *Phys. Rev. B* **102**, 140401(R) (2020).
- [52] Y. Yokoyama and C. Hotta, *Phys. Rev. B* **97**, 180404(R) (2018).
- [53] T. Hikihara, T. Misawa, and T. Momoi, *Phys. Rev. B* **100**, 214414 (2019).
- [54] K. Tanaka and C. Hotta, *Phys. Rev. B* **101**, 094422 (2020).
- [55] T. Sakai, T. Tonegawa, and K. Okamoto, *Phys. Status Solidi B* **247**, 583 (2010).
- [56] P. Nightingale, *J. Appl. Phys.* **53**, 7927 (1982).
- [57] I. Affleck, *Phys. Rev. Lett.* **62**, 474 (1989).
- [58] I. Affleck, *Phys. Rev. B* **43**, 3215 (1991).
- [59] A. M. Tsvetlik, *Phys. Rev. B* **42**, 10499 (1990).
- [60] T. Sakai and M. Takahashi, *Phys. Rev. B* **43**, 13383 (1991).
- [61] T. Sakai and M. Takahashi, *J. Phys. Soc. Jpn.* **60**, 3615 (1991).
- [62] A. Parvej and M. Kumar, *Phys. Rev. B* **96**, 054413 (2017).
- [63] D. Shanks, *J. Math. Phys.* **34**, 1 (1955).
- [64] M. N. Barber, in *Phase Transitions and Critical Phenomena* edited by C. Domb and J. M. Lebowitz (Academic Press, New York, 1983), p. 145.
- [65] H. Manaka, I. Yamada, and K. Yamaguchi, *J. Phys. Soc. Jpn.* **66**, 564 (1997).
- [66] H. Manaka, I. Yamada, Z. Honda, H. Aruga Katori, and K. Katumata, *J. Phys. Soc. Jpn.* **67**, 3913 (1998).
- [67] T. Masuda, A. Zheludev, H. Manaka, L.-P. Regnault, J.-H. Chung, and Y. Qiu, *Phys. Rev. Lett.* **96**, 047210 (2006).
- [68] V. O. Garlea, A. Zheludev, T. Masuda, H. Manaka, L.-P. Regnault, E. Ressouche, B. Grenier, J.-H. Chung, Y. Qiu, K. Habicht, K. Kiefer, and M. Boehm, *Phys. Rev. Lett.* **98**, 167202 (2007).
- [69] T. Hong, V. O. Garlea, A. Zheludev, J. A. Fernandez-Baca, H. Manaka, S. Chang, J. B. Leao, and S. J. Poulton, *Phys. Rev. B* **78**, 224409 (2008).
- [70] O. Vaccarelli, A. Honecker, P. Giura, K. Béneut, B. Fak, G. Rousse, and G. Radtke, *Phys. Rev. B* **99**, 064416 (2019).
- [71] O. Vaccarelli, G. Rousse, A. Saúl, and G. Radtke, *Phys. Rev. B* **96**, 180406(R) (2017).
- [72] H. Yamaguchi, H. Miyagai, Y. Kono, S. Kittaka, T. Sakakibara, K. Iwase, T. Ono, T. Shimokawa, and Y. Hosokoshi, *Phys. Rev. B* **91**, 125104 (2015).
- [73] H.-J. Grafe, S. Nishimoto, M. Iakovleva, E. Vavilova, L. Spillecke, A. Alfonsov, M.-I. Sturza, H. Nojiri, H. Rosner, J. Richter, U. K. Rößler, S.-L. Drechsler, V. Kataev, and B. Büchner, *Sci. Rep.* **7**, 6720 (2017).
- [74] S. C. Furuya, *Phys. Rev. B* **95**, 014416 (2017).
- [75] T. Sakai, *Phys. Rev. B* **57**, R3201 (1998).
- [76] R. Nakanishi, T. Yamada, R. Furuchi, H. Nakano, H. Kaneyasu, K. Okamoto, T. Tonegawa, and T. Sakai (unpublished).
- [77] T. Sakai, R. Furuchi, H. Nakano, and K. Okamoto (unpublished).